IEEE Access
Multidisciplinary ⋮ Rapid Review ⋮ Open Access Journal

Received 4 August 2023, accepted 9 September 2023, date of publication 15 September 2023, date of current version 21 September 2023.

Digital Object Identifier 10.1109/ACCESS.2023.3315149

RESEARCH ARTICLE

Innovative Fibromyalgia Detection Approach Based on Quantum-Inspired 3LBP Feature Extractor Using ECG Signal

PRABAL DATTA BARUA[1,2], MAKIKO KOBAYASHI[1,9], (Senior Member, IEEE), MASAYUKI TANABE[1], (Member, IEEE), MEHMET BAYGIN[3], JOSE KUNNEL PAUL[4], THOMAS IYPE[4], SENGUL DOGAN[5], TURKER TUNCER[5], RU-SAN TAN[6,7], AND U. RAJENDRA ACHARYA[8,9]

[1]Graduate School of Science and Technology, Kumamoto University, Kumamoto 860-8555, Japan
[2]School of Business (Information System), University of Southern Queensland, Toowoomba, QLD 4350, Australia
[3]Department of Computer Engineering, Faculty of Engineering and Architecture, Erzurum Technical University, 25050 Erzurum, Turkey
[4]Department of Neurology, Government Medical College Thiruvananthapuram, Thiruvananthapuram, Kerala 625020, India
[5]Department of Digital Forensics Engineering, Technology Faculty, Firat University, 23119 Elazig, Turkey
[6]Department of Cardiology, National Heart Centre Singapore, Singapore 169609
[7]Duke–NUS Medical School, Singapore 169857
[8]School of Mathematics, Physics and Computing, University of Southern Queensland, Springfield, QLD 4300, Australia
[9]International Research Organization for Advanced Science and Technology (IROAST), Kumamoto University, Kumamoto 860-8555, Japan

Corresponding author: Sengul Dogan (sdogan@firat.edu.tr)

ABSTRACT Fibromyalgia is a chronic pain syndrome associated with sleep disturbances, which may manifest as altered electroencephalography and electrocardiography (ECG) signal alterations during sleep. We aimed to develop a lightweight machine learning model for diagnosing fibromyalgia using single-lead ECG signals recorded during sleep. We analyzed 139 single-lead ECGs recorded during Stage 2 and Sleep Stage 3 of 16 patients with fibromyalgia and 16 age and sex matched controls. ECG records were divided into 15-second segments: 3308 and 1783 in healthy vs fibromyalgia classes, respectively. Our model comprised (1) feature extraction that combined an 8-wavelet filter and 4-level multiple filters-based multilevel discrete wavelet transform signal decomposition with a novel local binary pattern (LBP)-like function, 3LBP, that generated multiple patterns (analogous to quantum superposition) for feature map value extraction (the optimal input-specific pattern was dynamically selected using a novel forward-forward algorithm); (2) feature selection using neighborhood component analysis and Chi-square functions; (3) classification with k-nearest neighbors and support vector machine classifiers using leave-one-record-out cross-validation; and (4) mode function-based iterative majority voting to generate voted results, from which the best model result was derived. Our model attained binary classification accuracies of 93.87% and 92.02% for Sleep Stage 2 and Sleep Stage 3, respectively. The observed outcomes and empirical evidence unequivocally demonstrate the efficacy of our proposed methodology in differentiating the electrocardiographic signatures of fibromyalgia patients from control subjects. The model exhibited self-organizational properties and computational efficiency, rendering it amenable to facile clinical integration.

INDEX TERMS ECG-based fibromyalgia detection, 3LBP, multiple filters-based multilevel discrete wavelet transform, leave-one-record-out cross-validation, quantum-based feature extraction.

I. INTRODUCTION

A. BACKGROUND

Fibromyalgia, a chronic pain syndrome, is associated with pain [1], [2] in various body regions, especially in muscles, connective tissue, and around joints [3], as well as fatigue and difficulty with memory, concentration, and sleep [4], [5]. The cause of fibromyalgia is unclear, although genetic predisposition, physical or emotional trauma, various infections, and hormonal imbalances have been implicated as triggers [6], [7], which may vary among patients [8]. During the clinical evaluation of fibromyalgia, the usual procedure involves

The associate editor coordinating the review of this manuscript and approving it for publication was Anandakumar Haldorai.

reviewing symptoms, conducting a physical examination, and performing specific laboratory tests [9]. The diagnosis of fibromyalgia is challenging [10], and hinges crucially on a history of pain persistence in the absence of an identifiable medical cause [11]; specific laboratory or imaging diagnostic tests remain elusive. As definitive treatment for fibromyalgia is lacking [12], current management revolves around alleviating symptoms and enhancing patients' quality of life [13], i.e., symptom-relieving drugs, exercise, physical therapy, and sleep planning [14], which may need to be individualized depending on the different patterns of symptom presentation in individual patients [15].

A few researchers investigated the use of biomedical signals to facilitate the diagnosis of fibromyalgia [16], including analyses of continuous electroencephalograpram (EEG) and electrocardiography (ECG) signals recorded during sleep [17]. High data volume and temporal variations at different sleep stages render manual signal interpretation highly challenging [18]. This interpretative task may be posed as a classification challenge, for which automated artificial intelligence-enabled solutions may be applied [19]. For example, automated EEG- and ECG-based models have been proposed for the diagnosis of neurological [20] and cardiac [20], [21] conditions, respectively. In this study, we present a lightweight machine learning model for discriminating fibromyalgia vs healthy subjects using single-lead ECG signals recorded during sleep.

B. LITERATURE SURVEY

Disturbed sleep is a cardinal symptom of fibromyalgia. Thomas et al. [17] used spectrograms and statistical analyses to study EEG and ECG signals recorded during sleep from fibromyalgia and control subjects. They demonstrated that fibromyalgia-associated sleep instability induced perturbations consistently in both EEG and ECG signals, implying a heart-brain connection in the disease manifestation. Bilgin et al. [22] examined the correlation between heart rate variability, a marker of sympathetic nervous system activation [23], and anxiety levels in fibromyalgia patients using ECGs obtained from 56 fibromyalgia and 34 control subjects. The ECG signals were decomposed into sub-bands using wavelet packet transform and input to multilayer perceptron neural networks for classification. ECG-assessed heart rate variability parameters were shown to be useful for fibromyalgia diagnosis. Aksu et al. [16] studied the ECGs of 43 fibromyalgia and 30 control female subjects. From the analysis of parameters like fragmented QRS morphology, P dispersion, QT dispersion, as well as inter- and intra-atrial electromechanical delay, they found fibromyalgia patients more likely to have ECG changes that predisposed to atrial and ventricular arrhythmia. This pro-arrhythmia potential was corroborated in animal experiments by Nakata et al. [24], who showed that experimental high walking exercise loads could induce arrhythmia in mouse models of fibromyalgia.

C. LITERATURE GAP

While there is limited research on ECG-based fibromyalgia diagnosis, a few promising scientific insights have emerged, such as the association between fibromyalgia status and ECG signals [16], [22], and the correlation between sleep EEG-ECG signals in sleep-impaired fibromyalgia patients [17]. Additionally, few classification models have been developed for automated ECG-based fibromyalgia detection. Recognizing this gap, we aimed to create an accurate yet computationally efficient model for the high-throughput analysis of sleep ECG signals in diagnosing fibromyalgia. To achieve this, we used handcrafted multilevel dynamic feature engineering techniques. These techniques emulate the deep feature extraction and superior classification performance of deep learning networks, eliminating the need for time-consuming sequential weight optimization across different network layers.

D. MOTIVATIONS AND OUR MODEL

The heart-brain connection suggests that changes in biophysical signals like EEG and ECG may occur concomitantly in diseases that affect the nervous system primarily; this observation has been harnessed to advantage in computer-aided diagnosis of neurological diseases [25], including fibromyalgia [17]. Our research question is centered on demonstrating the feasibility of a computationally lightweight self-organized ECG signal-based handcrafted machine learning model for distinguishing ECG of fibromyalgia patients from healthy controls. To overcome the limited performance of non-deep learning models, we proposed innovative feature engineering methods. Our model comprised four phases: (1) feature extraction that combined multiple filters-based multilevel discrete wavelet transform (MFMDWT) preprocessing [26] with a novel local binary pattern (LBP) [27]-like textural feature generator, 3LBP; (2) feature selection by neighborhood component analysis (NCA) [28] and Chi-square (Chi2) [29] functions; (3) classification with standard shallow k-nearest neighbors (kNN) [30] and support vector machine (SVM) [31] classifiers; and (4) information fusion using mode function-based iterative majority voting (IMV) [32]. Of note, MFMDWT enabled multilevel feature extraction in both the spatial and frequency domains from the decomposed wavelet sub-bands. Additionally, the 3LBP-based feature generator incorporated a novel dynamic forward-forward (FF) feature map value selection operation that emulated the Hinton's FF algorithm [33] that was originally proposed for deep learning. The 3LBP generated multiple patterns per signal input, which is somewhat akin to the concept of quantum superposition: a quantum system can exist in multiple states at the same time until it is measured. We designed a straightforward FF operation inspired by Hinton's FF algorithm that dynamically selected from among those generated one optimal pattern specific to the input signal that could.be used for downstream textural feature extraction The FF strategy simulated human neural systems and was computationally less costly compared with ubiquitous backpropagation (which is unlikely to occur in nature [33]) seen with deep learning. Through dynamic input signal-specific feature extraction [19], we believed that quantum-based models could affect fast, comprehensive and deep characterization of data features that would enhance downstream model classification performance.

E. NOVELTIES

In this work, we proposed an innovative feature engineering model to detect fibromyalgia. The highlights of the work are as follows.

- Enhanced the standard multilevel discrete wavelet transform (MDWT) method for signal decomposition.
- Integrated multiple filters with unique attributes, facilitating the design of wavelet filters with diverse characteristics [34].
- Previously applied to one-dimensional sound signals [34], and in this work we applied it to the ECG signals.
- Introduced a custom 3LBP feature generator.
- Drawing inspiration from both quantum mechanics and Hinton's FF algorithm [33].
- Incorporated an optimal feature map value selection function, ensuring dynamic and input signal-specific feature extraction.

We improved the standard multilevel discrete wavelet transform-based signal decomposition by incorporating multiple filters with distinct properties, thereby allowing the creation of wavelet filters with a broad range of characteristics [34]. Previously applied to one-dimensional sound signals [34], MFMDWT was used for the first time in this study to analyze ECG signals. Our customized 3LBP feature generator incorporated a quantum- and Hinton's FF algorithm [33]-inspired optimal feature map value selection function that enabled dynamic and input signal-specific feature extraction.

F. CONTRIBUTIONS

The contributions of our proposal are as follows:

- Our model achieved outstanding binary classification accuracies of more than 92%.
- Employed leave-one-record-out (LORO) cross-validation (CV) approach [35].
- LORO CV considers differences among individual ECG records.
- This method is generalizable as we employed LORO CV using ECG signals.
- To the best of our knowledge, we are the first group to present an automated fibromyalgia detection system using ECG signals. We have employed the LORO CV and a self-organized feature engineering model in our study.
- Also, our model is computationally efficient, making it suitable for ECG-based clinical screening of fibromyalgia.

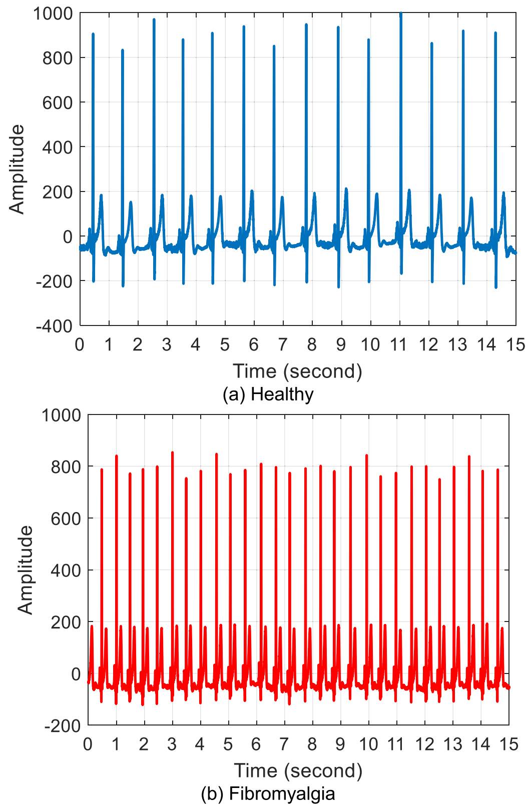

FIGURE 1. Example ECG signals used in the study dataset.

II. STUDY DATASET

We analyzed 139 single-lead ECGs recorded at Sleep Stage 2 and Sleep Stage 3 (which exemplify light sleep and non-rapid eye movement deep sleep, respectively) of polysomnographic sleep studies of 16 healthy subjects and 16 patients with fibromyalgia [36]. ECG signals were sampled at 512 Hz and stored as.edf files. These were converted to.mat files and divided into non-overlapping 15-second segments with 7680 data points (=15×512) each. We adopted a systematic naming convention for these mat files, which incorporated the sleep stage, class name, record number, and segment number. There were 3308 (=1811 + 1497) and 1783 (=1012 + 771) segments corresponding to the healthy and fibromyalgia classes, respectively (Table 1), examples of which are shown in Figure 1.

III. PROPOSED FEATURE ENGINEERING MODEL

Our feature engineering model encompassed several phases: feature extraction, feature selection, classification, and information fusion. Initially, input signals were decomposed using an 8-wavelet filter within a 4-level MFMDWT framework. Both the generated low-pass filter wavelet sub-bands and the raw ECG signal were then processed using the 3LBP textural

TABLE 1. **16-subject study ECG dataset stratified by Sleep Stage and Class.**

Sleep Stage	Class	ECG records (n)	ECG segments (n)
2	Healthy	42	1811
	Fibromyalgia	32	1012
3	Healthy	36	1497
	Fibromyalgia	26	771

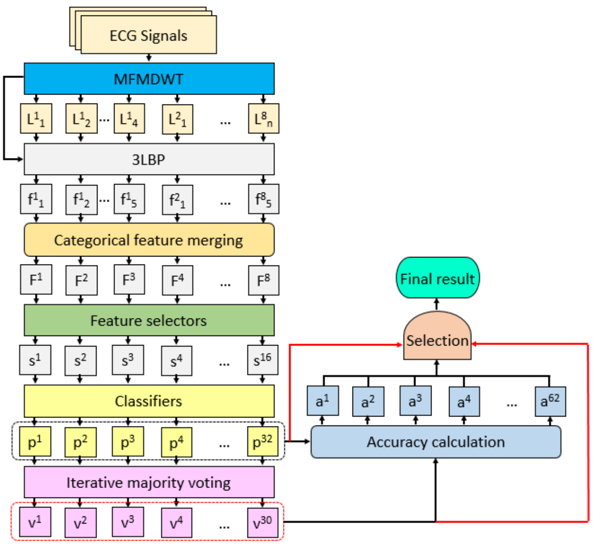

FIGURE 2. **Block diagram of the proposed feature engineering model. **w, wavelet sub-band; f, feature vector generated by 3LBP function; F, merged feature vector; s; selected feature vector; p, prediction vector; v, voted prediction vector; a, calculated accuracy.**

feature extraction function. This process yielded 40 feature vectors, each of length 256. These vectors were subsequently grouped according to their corresponding wavelet filter, consolidating them into 8 vectors, each of length 1280 (=256 × 5).

These consolidated vectors were introduced to NCA and Chi2 feature selectors. From each of these merged vectors, two refined feature vectors with reduced dimensionality were derived. Each of these vectors retained the most informative 256 features out of the initial set of 1280. Consequently, a sum of 16 (=8 × 2) selected feature vectors emerged. These were further input to kNN and SVM classifiers, producing 32 (=16 × 2) classifier-wise prediction vectors.

As a concluding step, IMV was applied to these 32 prediction vectors, generating an additional 30 voted prediction vectors. From the aggregated 62 (32 + 30) results, the prediction with the paramount classification accuracy was selected (refer to Figure 2). Comprehensive details of each phase will be expounded upon in the subsequent sections.

A. FEATURE EXTRACTION

The feature extraction architecture incorporated MFMDWT, facilitating multilevel feature generation from both the raw signal and its decomposed wavelet sub-bands. Additionally,

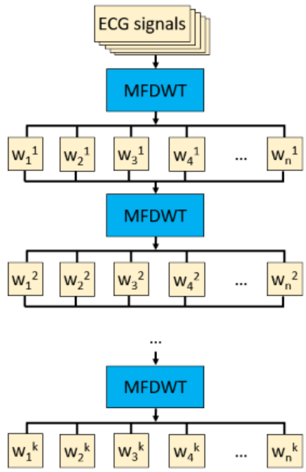

FIGURE 3. **Block diagram of the MFMDWT.**

the 3LBP method was used, which autonomously produced multiple patterns, akin to "quantum states." From these patterns, the optimal one specific to the input signal block was dynamically selected using an integrated handcrafted FF function. This function, reminiscent of Hinton's FF algorithm, was employed to derive map values for the creation of histogram-based feature vectors.

1) MULTIPLE FILTERS-BASED MULTILEVEL DISCRETE WAVELET TRANSFORM

The MFMDWT [34] enhances the traditional multilevel discrete wavelet transform by integrating multiple wavelet filters concurrently. This expands the selection of appropriate wavelet filter types for signal decomposition (refer to Figure 3), which could potentially lead to improved classification performance.

Equations (1) – (4) below defines MFMDWT-based signal decomposition into low- and high-pass wavelet sub-bands.

S1: Select wavelet filters.

S2: Input signal to the MFMDWT.

$$\left[low_1^i, high_1^i\right] = \delta\left(signal, ft^i\right), \quad i \in \{1, 2, \ldots, k\} \quad (1)$$

$$\left[low_{j+1}^i, high_{j+1}^i\right] = \delta\left(low_j^i, f^i\right), \quad j \in \{1, 2, \ldots, n\} \quad (2)$$

$$w_{2j-1}^i = low_j^i \quad (3)$$

$$w_{2j}^i = high_j^i \quad (4)$$

where *low* represents low-pass filter band; *high*, high-pass filter band; $\delta(.,.)$, discrete wavelet transform function; *ft*, wavelet filter; *k*, number of wavelet filters; and *n*, number of levels.

2) 3LBP: A QUANTUM-INSPIRED FEATURE EXTRACTION FUNCTION

For each input signal block, the 3LBP function produced nine distinct patterns. To identify the optimal pattern specific to the input signal, we developed a handcrafted FF pattern

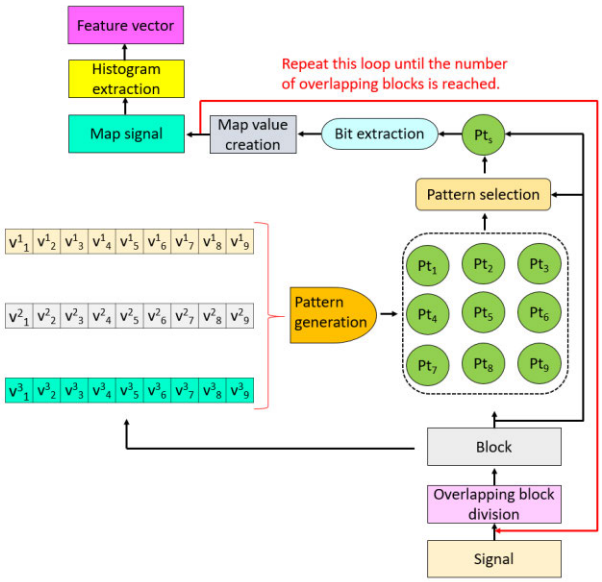

FIGURE 4. **Block diagram of the 3LBP feature extraction function. **Pt, pattern; Pts, selected pattern; v, value within each signal block.**

selection algorithm, drawing inspiration from Hinton's FF algorithm [33] (Figure 4).

The 11 steps below define the proposed quantum-inspired 3LBP feature extraction function.

S1: Calculate the mean value of the signal.

$$mv = \frac{1}{\mathcal{L}} \sum_{q=1}^{\mathcal{L}} signal(q) \tag{5}$$

where mv represents the mean value of the signal; and $\mathcal{L}$, signal length.

S2: Divide the signal into overlapping blocks of length 27.

$$bl^h(t) = signal(h+t-1), \quad h \in \{1, 2, \ldots, L-26\}, \quad t \in \{1, 2, \ldots, 27\} \tag{6}$$

where bl^h, represents h[th] overlapping block of length 27.

S3: Create sub-blocks from the block generated in S2.

$$b_a(x + 9 \times (a-1)) = bl^h(x), \quad x \in \{1, 2, \ldots, 9\}, \quad a \in \{1, 2, 3\} \tag{7}$$

where b represents the sub-block. Here, three sub-blocks were created.

S4: Create nine groups using the three sub-blocks created in S3.

$$gr_a = b_a \tag{8}$$
$$gr_4(ngh(e)) = b_1(ngh(e)), \quad gr_4(5) = b_2(5), \tag{9}$$
$$gr_5(ngh(e)) = b_1(ngh(e)), \quad gr_5(5) = b_3(5) \tag{10}$$
$$gr_6(ngh(e)) = b_2(ngh(e)), \quad gr_6(5) = b_3(5) \tag{11}$$
$$gr_7(ngh(e)) = b_2(ngh(e)), \quad gr_7(5) = b_1(5) \tag{12}$$
$$gr_8(ngh(e)) = b_3(ngh(e)), \quad gr_8(5) = b_1(5) \tag{13}$$
$$gr_9(ngh(e)) = b_3(ngh(e)), \quad gr_9(5) = b_2(5) \tag{14}$$
$$ngh \in \{1, 2, \ldots, 9\} \text{ and } ngh \neq 5, \quad e \in \{1, 2, \ldots, 8\} \tag{15}$$

where ngh represents the index of the neighbor value; gr, group.

S5: Calculate the mean value of each group.

$$gmv_b = \frac{1}{9} \sum_{i=1}^{9} gr_b(i), \quad b \in \{1, 2, \ldots, 9\} \tag{16}$$

where gmv represents the mean value of each group. Here, nine mean values were calculated.

S6: Calculate differences in the mean values.

$$dif_b = |mv - gmv_b| \tag{17}$$

where dif represents the calculated difference.

S7: Find the index of the minimum distance.

$$id = \min(dif) \tag{18}$$

where id represents the index of the minimum difference.

Equations (16) - (18) define the novel FF mean value-based group selection method to select the optimal group (pattern) for downstream textural feature extraction.

S8: Extract binary features by applying the signum function to the selected index.

$$bit(e) = signum(gr_{id}(ngh(e)), gr_{id}(5)) \tag{19}$$

$$signum(gr_{id}(ngh(e)), gr_{id}(5)) = \begin{cases} 0, & gr_{id}(ngh(e)) - gr_{id}(5) < 0 \\ 1, & gr_{id}(ngh(e)) - gr_{id}(5) \geq 0 \end{cases} \tag{20}$$

where bit represents generated binary values.

S9: Compute map value using the 8 bits generated in S8.

$$map(h) = \sum_{e=1}^{8} bit(e) \times 2^{e-1} \tag{21}$$

S10: Repeat S2-S9 for the number of overlapping blocks in the signal to generate the map signal.

S11: Extract histogram of the map signal to generate feature vector.

$$fv = \eta(map) \tag{22}$$

where fv represent generated feature vector of length 256 ($= 2^8$); and η, histogram extraction function.

3) STEPS OF THE PROPOSED FEATURE EXTRACTION METHOD

The steps for feature extraction in our model, based on MFMDWT and 3LBP, are outlined below.

Step 1: The generic MFMDWT function is defined in Section III-A1. To ensure a comprehensive coverage of wavelet domains in our model, we employed eight renowned filters: Haar, Daubechies 4 (db4), Coiflet 4 (coif4), Symlet 4, Fejér-Korovkin 6 (fk6), Discrete Meyer (dmey), BiorSplines 3.5 (bior3.5), and Reverse Bior 3.5 (rbior3.5). Additionally, the MFMDWT was executed at four levels of signal decomposition, using low-pass filters to produce wavelet sub-bands for subsequent feature extraction.

$$\left[low_1^i, high_1^i\right] = \delta\left(signal, ft^i\right), \quad i \in \{1, 2, \ldots, 8\} \tag{23}$$

$$\left[low_{j+1}^i, high_{j+1}^i\right] = \delta\left(low_j^i, f^i\right), \quad j \in \{1, 2, 3, 4\} \tag{24}$$

Step 2: Both the raw ECG signal and the derived low-pass wavelet sub-bands were fed into the proposed 3LBP-based feature extractor.

$$f_1^i = \alpha(signal) \tag{25}$$

$$f_{j+1}^i = \alpha(low_j^i) \tag{26}$$

where $\alpha(\cdot)$ represents the 3LBP feature extraction function (the detailed steps are defined in Section III-A2); and f, extracted feature vectors of length 256.

Step 3: Concatenate the generated feature vectors categorically based on the wavelet filter used.

$$\begin{aligned} F^i\left(r + 256 \times (b-1)\right) &= f_b^i(r), \quad r \in \{1, 2, \ldots, 256\}, \\ & b \in \{1, 2, \ldots, 5\}, \quad i \in \{1, 2, \ldots, 8\} \end{aligned} \tag{27}$$

where F denotes the merged feature vector. We generated eight merged feature vectors, each of length 1280, facilitating a comprehensive survey of signal data characteristics specific to each wavelet filter. These characteristics had been previously segmented into multiple frequency domains.

B. MULTIPLE SELECTORS-BASED FEATURE SELECTION

We deployed standard NCA [28] and Chi2 [29] feature selection functions in our model. NCA assigns positive weights to features based on their distance-related importance to select the most informative features, while Chi2 employs the Chi-squared statistical metric. Both methods enable the efficient identification of the most discriminative features, considerably reducing data dimensionality. From the eight merged feature vectors, each of length 1280, NCA and Chi2 produced 16 feature vectors, each spanning 256 units in length.

To elucidate the feature selection process using multiple selectors, we detail the steps of this phase below.

Step 4: Generate qualified indexes of all features by deploying NCA and Chi2 feature selectors.

$$ind_i^N = \mu\left(F^i, y\right) \tag{28}$$

$$ind_i^C = \chi\left(F^i, y\right) \tag{29}$$

where ind^N represents qualified index generated by NCA; ind^C, qualified index generated by Chi2; $\mu(.,.)$, NCA feature selection function; $\chi(.,.)$, Chi2 feature selection function; and y, output.

Step 5: Create 16 selected feature vectors using both NCA- and Chi2-generated indexes.

$$s_i(d, c) = F^i\left(d, ind_i^N(c)\right), \quad d \in \{1, 2, \ldots, N\},$$

$$c \in \{1, 2, \ldots, 256\} \tag{30}$$

$$s_{i+8}(d, c) = F^i\left(d, ind_i^C(c)\right) \tag{31}$$

where s represents the selected feature vector of length 256; and N, the number of observations.

C. CLASSIFICATION

The 16 selected feature vectors were fed into the established and effective shallow kNN [30] and SVM [31] classifiers. Utilizing the LORO CV strategy, we employed the fine kNN and quadratic SVM within the MATLAB Classification Learner Toolbox, deriving two classifier-specific outcomes for each selected feature vector. An explanation of these classifiers is provided below.

1) kNN [30]

kNN is a non-parametric, instance-based classifier. It classifies a data based on how its neighbors are classified. When a data needs to be classified, the algorithm looks for the 'k' nearest data point (where 'k' is a user-defined parameter) and assigns a label based on the majority class of those neighbors. kNN is simple, intuitively easy to understand, and is generally effective for datasets where data points close to the feature space have the same label. It is computationally intensive for large datasets, sensitive to unrelated features, and can be distorted by unstable datasets.

2) SVM [31]

SVM is a supervised learning algorithm. Its primary function is to find a hyperplane that best divides a data into classes; This makes it particularly effective in high-dimensional spaces and where there is a clear margin of separation. One of the advantages is its effectiveness in these high-dimensional spaces. It can also use a subset of training points, known as support vectors, in the decision function and is versatile due to its ability to use different kernel functions for data separation. The selection of an appropriate kernel function is crucial and the algorithm may become less effective if there is a significant amount of noise in the dataset.

The hyperparameters used for various classifiers are tabulated in Table 2.

Step 6: Classify the 16 selected feature vectors by deploying kNN and SVM classifiers.

$$p_t = kNN(s_t, y), \quad t \in \{1, 2, \ldots, 16\} \tag{32}$$

$$p_{t+16} = SVM(s_t, y) \tag{33}$$

where p represents the prediction vector. 32 prediction vectors were generated from the 16 selected feature vectors.

D. INFORMATION FUSION

We utilized the mode function-based IMV [32] to produce voted prediction vectors. With the iteration range set from 3 (the minimum number of vectors required for mode function-based selection) to 32 (the total number of classifier-wise prediction vectors), we generated an additional 30 voted prediction vectors. Each of these vectors was derived from an array of the top classifier-specific outcomes, representing the collective decision-making process. We computed the classification accuracies for each of the classifier-specific prediction vectors as well as the IMV-voted prediction vectors, comparing them. The result with the highest accuracy was chosen as the model's final outcome. This information fusion facilitated a self-organized determination of the model's optimal result. The steps are detailed further below.

Step 7: Deploy IMV to calculated voted prediction vectors.

$$v = \varpi(p) \tag{34}$$

where $\varpi(\cdot)$ represents IMV function; and v, voted prediction vector. Here, 30 voted prediction vectors were generated from 32 classifier-wise prediction vectors.

Step 8: Select the most accurate result as the final result according to classification accuracy.

$$ac_w = \phi(p_w), \quad w \in \{1, 2, \ldots, 32\} \tag{35}$$

$$ac_{g+32} = \phi(v_g), \quad g \in \{1, 2, \ldots, 30 \tag{36}$$

$$indx = \max(ac) \tag{37}$$

$$fres = \begin{cases} p_{indx}, & indx \leq 32 \\ v_{inx-32}, & indx > 32 \end{cases} \tag{38}$$

where $\phi(\cdot)$ represents the accuracy calculation function; ac, classification accuracy; $indx$, index of the output with maximum accuracy; and $fres$, final result.

Steps 1-8 above define our ECG signal classification model for fibromyalgia detection.

IV. EXPERIMENTAL RESULTS

The model was developed and implemented in MATLAB (2020a) programming environment on a personal computer with a 3.6 GHz central processing unit, 64 GB memory, and Windows 10 Professional operating system. The parametric model settings are detailed in Table 2.

Standard evaluation metrics were used to assess the model's performance: accuracy, specificity, sensitivity, and geometric mean. The mathematical definitions are listed below.

$$ac = \frac{tp + tn}{tp + fn + fp + tn} \tag{39}$$

$$sp = \frac{tn}{fp + tn} \tag{40}$$

$$sn = \frac{tp}{fn + tp} \tag{41}$$

$$gm = \sqrt{\frac{tn}{fp + tn} \times \frac{tp}{fn + tp}} \tag{42}$$

where ac represents accuracy; sp, specificity; sn, sensitivity; gm, geometric mean; tn, true negative; tp, true positive; fn, false negative; and fp, false positive.

A. CLASSIFIER-WISE RESULTS

We stratified the results by sleep stage. Our model attained excellent classification results for ECG signals acquired at Sleep Stage 2 (Table 3) and Sleep Stage 3 (Table 4). The highest classification accuracy of 93.20% at Sleep Stage 2 (light sleep) was attained by the 29th prediction vector (wavelet

TABLE 2. Parameter settings of proposed model.

Phase	Method	Input	Output	Parameter
Feature generation	MFMDWT	ECG signal	32 wavelet bands.	8 wavelet filters; number of levels: 4
	3LPB-based feature vector extraction	ECG signal and generated 32 wavelet sub-bands	40 feature vectors	Length of overlapping block: 27; bit extraction function: signum; number of patterns: 9; selection: mean differences-based algorithm; length of feature vector: 256
	Categorical merging	40 feature vectors	8 merged feature vectors	Length of each merged feature vector: 1280
Feature selection	NCA	8 merged feature vectors	8 selected feature vectors	Length of each selected feature vector: 256
	Chi2	8 merged feature vectors	8 selected feature vectors	Length of each selected feature vector: 256
Classification	kNN	16 selected feature vectors	16 kNN results	k:1; distance: L2-norm (Euclidean); voting: none; validation: LORO CV
	SVM	16 selected feature vectors	16 SVM results	Kernel: 2nd polynomial order; kernel scale: automatic; box constraint: 1.
Information fusion	IMV	32 classifier-wise results	30 voted results	Iteration range: 3 to 32; sort criteria: descending; voting function: mode.
	Selection of final result	62 results	1 result	Selection: maximum calculated accuracy

TABLE 3. Classifier-wise results for Sleep Stage 2.

No.	Ac (%)	Sp (%)	Sn (%)	Gm (%)
1	90.72	87.69	96.15	91.82
2	92.35	88.68	98.91	93.66
3	92.84	89.51	98.81	94.05
4	93.16	**90.39**	98.12	94.18
5	89.90	86.14	96.64	91.24
6	92.67	89.73	97.92	93.74
7	92.21	89.56	96.94	93.18
8	90.58	86.31	98.22	92.07
9	86.72	86.36	87.35	86.86
10	87.81	87.63	88.14	87.89
11	89.98	89.07	91.60	90.32
12	88.91	87.41	91.60	89.48
13	88.49	86.14	92.69	89.35
14	89.27	88.24	91.11	89.66
15	89.87	89.56	90.42	89.99
16	89.02	87.19	92.29	89.70
17	89.30	87.41	92.69	90.01
18	91.04	86.47	**99.21**	92.62
19	92.63	89.40	98.42	93.80
20	91.96	89.12	97.04	92.99
21	90.68	86.86	97.53	92.04
22	92.03	88.51	98.32	93.29
23	90.65	86.80	97.53	92.01
24	90.83	86.42	98.72	92.36
25	90.97	87.96	96.34	92.06
26	92.28	88.85	98.42	93.51
27	92.49	89.62	97.63	93.54
28	90.72	86.86	97.63	92.09
29	**93.20**	89.90	99.11	**94.39**
30	92.74	90.06	97.53	93.72
31	90.97	88.51	95.36	91.87
32	90.54	87.36	96.25	91.69
Mean	90.86	88.12	95.77	91.85

** Ac: accuracy; Sp: specificity; Sn: sensitivity; Gm: geometric mean.

filter: fk6; feature selector: Chi2; classifier: SVM) (Table 3); and of 90.26% at Sleep Stage 3 (deep sleep), by the 31st prediction vector (wavelet filter: bior3.5; feature selector: Chi2; classifier: SVM) (Table 4).

B. MAJORITY VOTING RESULTS

Our model attained excellent voted classification results for ECG signals acquired at Sleep Stage 2 (Table 5) and Sleep Stage 3 (Table 6) that surpassed the classifier-wise results. In the information fusion phase, the highest classification accuracy of 93.87% at Sleep Stage 2 (light sleep) was attained by the 8th-voted prediction vector (majority voting of the following ten classifier-wise prediction vectors in descending order of accuracy: a, b, c, d, e, f, g, h, i, j) (Table 5); and of 92.02% at Sleep Stage 3 (deep sleep), by the 7th voted prediction vector (majority voting of the following nine classifier-wise prediction vectors in descending order of accuracy: A, B, C, D, E, F, G, H, I) (Table 6).

C. FINAL RESULTS

Based on the highest calculated accuracy, the final results of our model are shown in Table 7. The corresponding confusion matrixes demonstrated overall acceptable rates of misclassification, with false positive rates of 14.2% and 5.8% for Sleep Stage 2 and Sleep Stage 3, respectively, and false negative rates of 0.4% and 8.9% for Sleep Stage 2 and Sleep Stage 3, respectively (Figure 5).

TABLE 4. Classifier-wise results for Sleep Stage 3.

No.	Ac (%)	Sp (%)	Sn (%)	Gm (%)
1	84.57	89.31	75.36	82.04
2	87.39	95.66	71.34	82.61
3	90.12	94.32	81.97	87.93
4	85.32	90.71	74.84	82.39
5	86.29	94.12	71.08	81.79
6	89.55	96.39	76.26	85.74
7	86.42	94.19	71.34	81.97
8	89.42	96.26	76.13	85.61
9	89.81	95.99	77.82	86.43
10	85.89	90.85	76.26	83.24
11	89.37	**96.66**	75.23	85.27
12	87.30	95.99	70.43	82.22
13	89.29	96.06	76.13	85.52
14	88.14	95.99	72.89	83.65
15	88.27	96.46	72.37	83.55
16	87.65	95.32	72.76	83.28
17	84.30	87.51	78.08	82.66
18	83.29	86.97	76.13	81.37
19	87.70	89.98	**83.27**	86.56
20	84.22	87.44	77.95	82.56
21	81.79	87.17	71.34	78.86
22	85.71	90.51	76.39	83.16
23	83.82	87.58	76.52	81.86
24	85.19	87.11	81.45	84.23
25	90.08	94.12	82.23	**87.98**
26	86.29	88.38	82.23	85.25
27	85.45	87.91	80.67	84.21
28	83.51	88.91	73.02	80.58
29	84.79	87.58	79.38	83.38
30	86.07	90.71	77.04	83.60
31	**90.26**	96.46	78.21	86.86
32	88.80	91.85	82.88	87.25
Mean	86.75	92.01	76.53	83.86

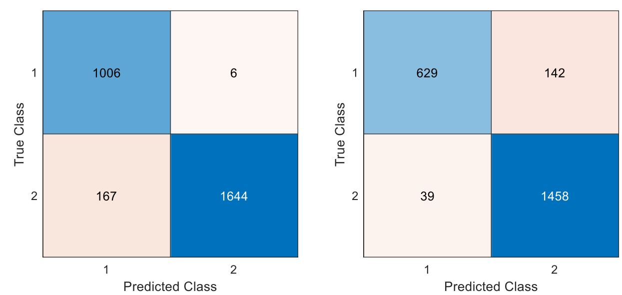

(a) Sleep Stage 2 (b) Sleep Stage 3

FIGURE 5. Confusion matrixes based on final model classification results, **Pt, pattern; Pts, selected pattern; v, value within each signal block. **Classes: 1, fibromyalgia; 2, healthy.

V. DISCUSSION

Our quantum-inspired ECG classification model attained excellent binary classification accuracy rates of >92% for discrimination of fibromyalgia vs healthy classes using single-lead ECG signals acquired during light (Sleep Stage 2) and deep (Sleep Stage 3). Notably, the results were attained

TABLE 5. Voted results for sleep stage 2.

No.	Ac (%)	Sp (%)	Sn (%)	Gm (%)
1	93.48	90.34	99.11	94.62
2	93.77	**90.94**	98.81	94.80
3	93.69	90.56	99.31	94.83
4	93.77	90.78	99.11	94.85
5	93.73	90.50	**99.51**	94.90
6	93.77	90.67	99.31	94.89
7	93.66	90.45	99.41	94.82
8	**93.87**	90.78	99.41	**94.99**
9	93.73	90.50	99.51	94.90
10	93.80	90.67	99.41	94.94
11	93.66	90.45	99.41	94.82
12	93.62	90.45	99.31	94.77
13	93.59	90.34	99.41	94.76
14	93.62	90.39	99.41	94.79
15	93.34	89.95	99.41	94.56
16	93.38	90.06	99.31	94.57
17	93.20	89.73	99.41	94.44
18	93.23	89.78	99.41	94.47
19	93.16	89.67	99.41	94.42
20	93.27	89.84	99.41	94.50
21	93.27	89.84	99.41	94.50
22	93.27	89.90	99.31	94.48
23	93.27	89.90	99.31	94.48
24	93.34	90.01	99.31	94.54
25	93.34	90.01	99.31	94.54
26	93.41	90.23	99.11	94.56
27	93.34	90.06	99.21	94.52
28	93.41	90.23	99.11	94.56
29	93.34	90.12	99.11	94.51
30	93.45	90.34	99.01	94.57
Mean	93.49	90.25	99.30	94.66

TABLE 6. Voted results for sleep stage 3.

No.	Ac (%)	Sp (%)	Sn (%)	Gm (%)
1	91.80	96.66	**82.36**	**89.22**
2	91.67	97.26	80.80	88.65
3	91.84	97.19	81.45	88.98
4	90.61	97.33	77.56	86.88
5	91.84	97.33	81.19	88.90
6	91.36	**97.39**	79.64	88.07
7	**92.02**	97.39	81.58	89.14
8	91.40	97.39	79.77	88.14
9	91.40	97.39	79.77	88.14
10	91.36	97.39	79.64	88.07
11	91.45	97.39	79.90	88.21
12	90.48	97.39	77.04	86.62
13	90.61	97.33	77.56	86.88
14	89.59	97.39	74.45	85.15
15	89.64	97.39	74.58	85.23
16	89.64	97.39	74.58	85.23
17	90.39	97.39	76.78	86.48
18	89.90	97.39	75.36	85.67
19	90.48	97.33	77.17	86.67
20	90.48	97.33	77.17	86.67
21	90.61	97.33	77.56	86.88
22	90.39	97.33	76.91	86.52
23	91.09	97.26	79.12	87.72
24	90.65	97.39	77.56	86.91
25	91.01	97.26	78.86	87.58
26	90.74	97.26	78.08	87.14
27	90.61	96.86	78.47	87.18
28	90.43	96.93	77.82	86.85
29	89.99	96.13	78.08	86.63
30	89.68	96.13	77.17	86.13
Mean	90.77	97.21	78.27	87.22

using robust LORO CV, which by aligning the fold count with the record count (there were a total of 139 ECG recordings in the dataset), was of greater relevance for the diagnostic assessment of individual ECG records than the conventional k-fold random splitting of ECG segments.

The model analyzed 15-second ECG segments (data length 7680), which were each divided into 7654 ($=7680 - 27 + 1$) overlapping signal blocks (data length 27) to feed to the 3LBP feature extractor. Nine patterns were generated by the quantum-inspired 3LBP function, from which only one was dynamically selected, using a mean distance-based FF algorithm, to extract map values from each input signal block. Figure 6 depicts an example of the frequency distribution of individual patterns used to process one ECG segment.

Our model generated 32 ($=8 \times 2 \times 2$) classifier-wise prediction vectors, each of which was the product of sequential processing by one each of eight wavelet filters, two feature selectors, and two classifier options. To assess the relative contributions of different wavelet sub-band, wavelet filters, feature selectors, and classifier options on classification performance, we stratified the results according to various utilized parameter options. For the best-performing 29th (wavelet filter: fk6; feature selector: Chi2; classifier: SVM) and 31st (wavelet filter: bior3.5; feature selector: Chi2; classifier: SVM) prediction vectors at Sleep Stage 2 and Sleep Stage 3, respectively (Tables 3 and 4), raw ECG signals contributed the most to the corresponding selected feature vectors (and thence classifier-wise results), although the cumulative contributions of all four wavelet sub-bands were 165 and 166 features out of 256 selected features for Sleep Stage 2

TABLE 7. Final model classification results stratified by sleep stages.

Sleep stage	Accuracy (%)	Specificity (%)	Sensitivity (%)	Geometric mean (%)
2	93.87	90.78	99.41	94.99
3	92.02	97.39	81.58	89.14

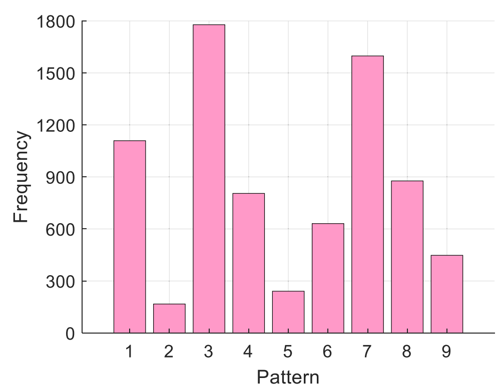

FIGURE 6. Frequency distribution of 3LBP-generated patterns used for an example ECG segment.

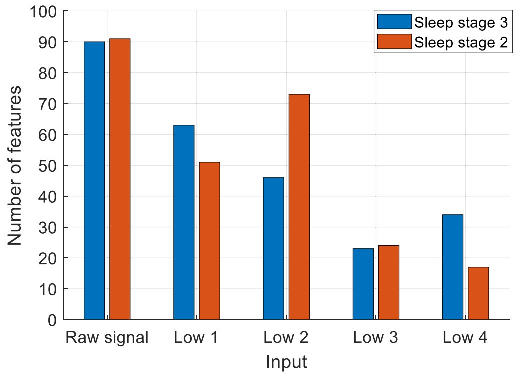

FIGURE 7. Frequency distribution raw ECG signal vs wavelet sub-band input contributing to the selected feature vectors that yielded the most accurate classifier-wise prediction vectors for both sleep stages.

and Sleep Stage 3, respectively (Figure 7). The latter observation underscores the value-add of the multilevel discrete wavelet transform in our model. Figure 8 and Figure 9 depict the differential contributions of the various classifiers, feature selectors and wavelet filters to classifier-wise results, expressed in terms of mean accuracies, in Sleep Stage 2 and Sleep Stage 3, respectively. For Sleep Stage 2, coif4 wavelet filter, NCA feature selector, and SVM yielded the highest classification ability (Figure 8); and for Sleep Stage 3, coif4, Chi2, and kNN (Figure 9).

Comparing the accuracy rates of classifier-wise and voted results for Sleep Stage 2 vs Sleep Stage 3, except for the 9th and 13th classifier-wise prediction vectors, all Sleep Stage 2 accuracy results surpassed those of Sleep Stage 3 (Figure 10), by as much as 1.85% (= 93.87% − 92.02%) (Table 7).

A. ABLATION STUDY

To examine the impact of 3LBP and LORO CV on model performance, we performed an ablation study using a simplified base model. We compared the 3LBP model with standard one-dimensional LBP [37] by applying these feature extractors to Sleep Stage 2 raw ECG signals and inputting the extracted features to the kNN classifier for classification using a 10-fold cross-validation strategy. 3LBP outperformed LBP, with accuracies of 98.94% and 95.71%, respectively. These results were also superior to those obtained with LORO CV. To examine this further, we re-analyzed the classifier-wise prediction vector results of our full MFMDWT-3LBP model for Sleep Stage 2 and Sleep Stage 3 using a 10-fold CV instead of a LORO CV. With a 10-fold CV, all classifier-wise results surpassed 99% accuracy for both sleep stages, with some even attaining 100% classification accuracy (Figure 11). Nevertheless, we remained convinced that LORO CV was the more rigorous standard, as well as more relevant and applicable for clinical fibromyalgia detection using ECG records.

Moreover, we have compared the classifiers using the best feature vectors of the sleep stage 2 and 3 stages. We have obtained these results using 10-fold CV. The computed classification performances of the classifiers are shown in Figure 12. Figure 12 demonstrated that the best classifiers are the kNN and SVM as they yielded the classification accuracy of above 99.5%.

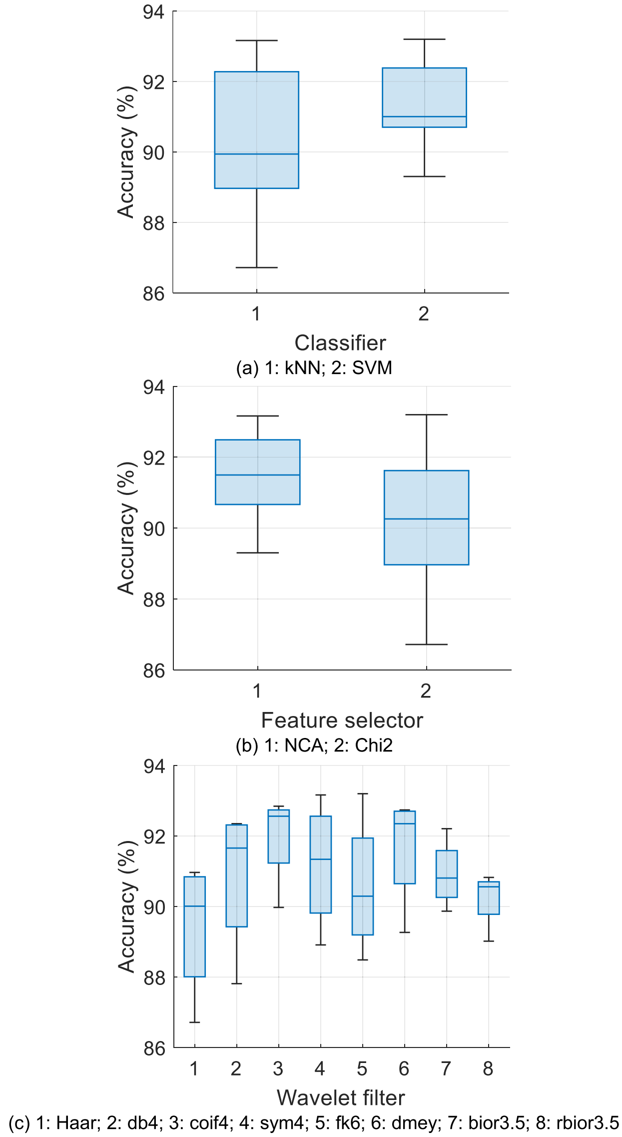

FIGURE 8. Mean accuracies of classifier-wise prediction vectors stratified by (a) classifier, (b) feature selector, and (2) wavelet filter using Sleep 2 ECG signals.

B. HIGHLIGHTS

Highlights of our research are listed below.

Findings:

- Overall, for Sleep Stage 2, the most effective wavelet filter, feature selector, and classifier were coif4, NCA, and SVM, respectively; and for Sleep Stage 3, coif4, Chi2, and kNN, respectively.
- The best individual classifier-wise results for Sleep Stage 2 and Sleep Stage 3 were obtained using fk6

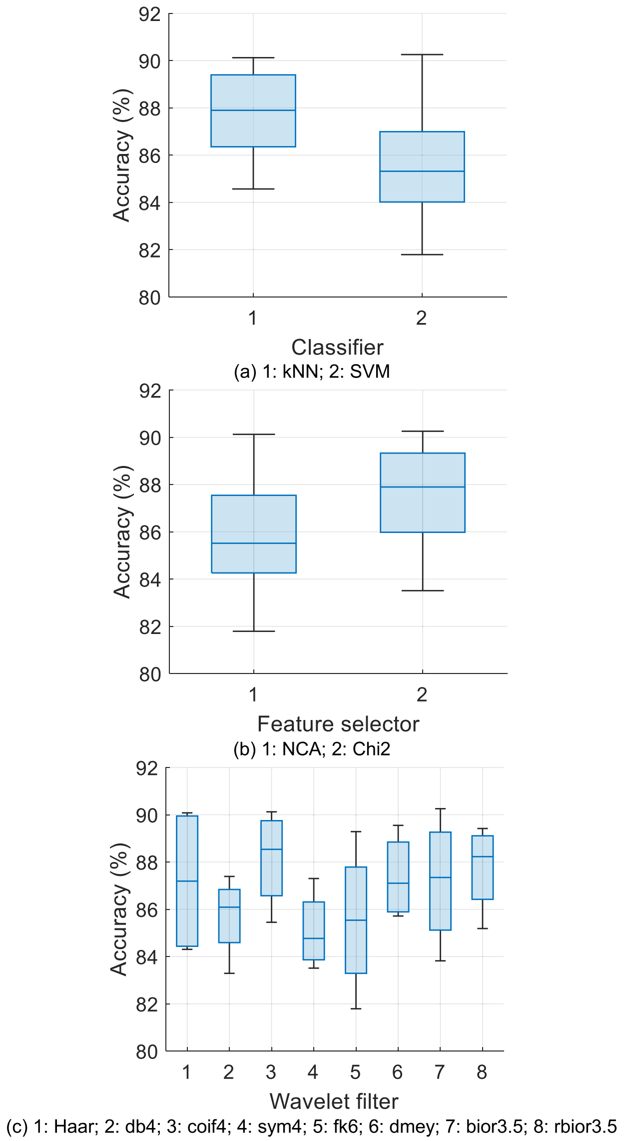

FIGURE 9. **Mean accuracies of classifier-wise prediction vectors stratified by (a) classifier, (b) feature selector, and (2) wavelet filter using Sleep 2 ECG signals.**

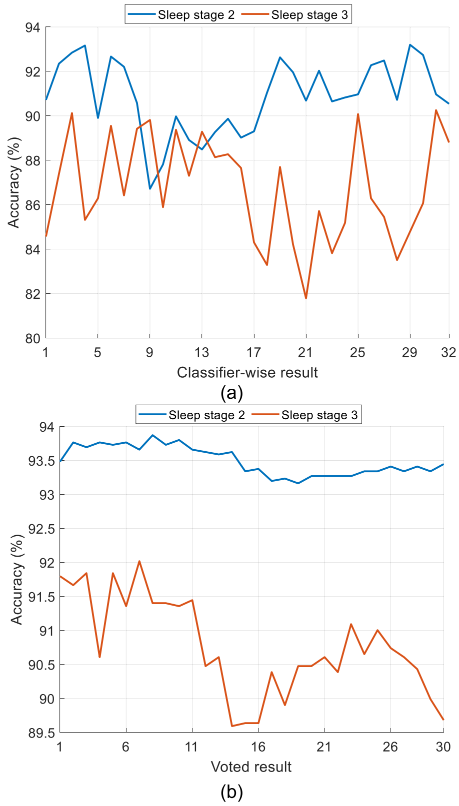

FIGURE 10. **Accuracies of (a) individual classifier-wise prediction vectors, and (b) voted prediction vectors, stratified by sleep stage.**

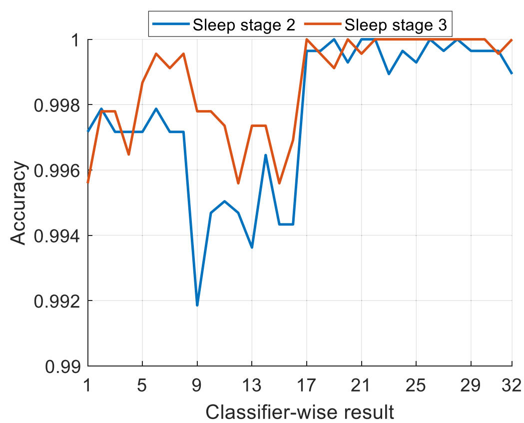

FIGURE 11. **Classifier-wise prediction vector accuracy results analyzed using 10-fold CV.**

and bior3.5 filters, respectively, coupled with the Chi2 feature selector and SVM classifier for both sleep stages.

- The final results obtained via voting surpassed classifier-wise results

Advantages:

- Our proposal has shown that ECG signals obtained from fibromyalgia patients can be effectively distinguished from those of healthy controls, indicating the significant influence of the disease on the autonomic nervous system, either as a primary factor or as a result of the pain that accompanies the condition.
- We introduced a novel feature extraction function, 3LBP, that was based on and, in an ablation study, surpassed LBP textural feature extraction (Section V-A).
- The excellent performance of 3LBP showcased the potential for deep feature generation using integrated dynamic and signal input-specific feature map value extraction, which was inspired by both quantum superposition and FF neural networks.
- Trained and validated using robust LORO CV, our model results were excellent (>92% accuracy for both sleep stages), generalizable, and clinically applicable. 10-fold CV-based results are also provided for reference (Section V-A).

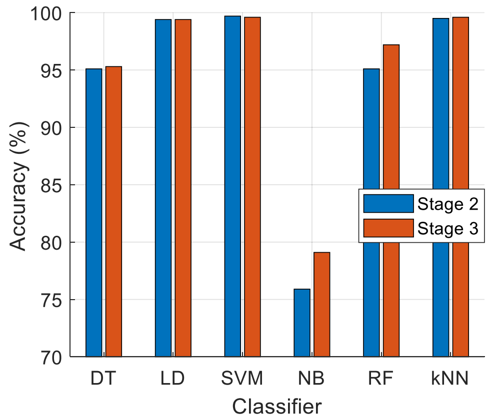

FIGURE 12. Performance comparisons of the classifiers. Herein, DT: Decision Tree, LD: Linear Discriminant, SVM: Support Vector Machine, NB: Naïve Bayes, RF: Random Forest, kNN: k Nearest Neighbor.

- The model is self-organized and can automatically calculate the best overall result.
- The model architecture is lightweight, which should enhance the ease of its clinical implementation.

Disadvantages:

- Our dataset was relatively modest. The findings should preferably be replicated on a larger and more diverse ECG signal dataset.
- We employed a simple mean absolute difference-based optimal pattern selection algorithm for 3LBP. Alternative mathematical models could be explored.
- Ideally, our future objective is to replicate the study by comparing the ECG signals of fibromyalgia patients with those of individuals who have other chronic painful medical conditions, matching them in terms of age, sex, and pain scores. By doing so, we can determine if the changes observed in the ECG signals are specific to fibromyalgia or if they are present in other similar conditions.

VI. CONCLUSION

In this study, we developed a new model for classifying ECG signals from fibromyalgia patients and healthy controls. Our model is based on quantum-inspired 3LBP (local binary patterns) and is a self-organized feature engineering model. We evaluated our model using LORO cross-validation and achieved classification accuracies of over 92% for both sleep stages 2 and 3. We also identified the optimal configurations of wavelet filters, feature selectors, and classifiers for each sleep stage. These findings demonstrate the effectiveness of our model for detecting and distinguishing ECG signals from fibromyalgia and healthy control patients.

In future works, we aim to expand the scale and diversity of our dataset. Building upon the foundation of our quantum-based model, our focus will shift towards exploring alternative mathematical models, feature selectors, and feature extractors to develop more effective ECG signal-based classification models.

Declarations

Funding: This research received no external funding.

Conflicts of Interest: The authors declare no conflict of interest.

Institutional Review Board Statement: Not applicable.

Informed Consent Statement: Not applicable.

Data Availability Statement: This dataset is available for download at [36].

REFERENCES

[1] M. M. Cristancho, G. B. Subieta, and M. L. Torres, "Myofascial pain syndrome and fibromyalgia," in *Chronic Pain Management in General and Hospital Practice*. Singapore: Springer, 2021, pp. 355–371.

[2] M.-A. Fitzcharles, S. P. Cohen, D. J. Clauw, G. Littlejohn, C. Usui, and W. Häuser, "Chronic primary musculoskeletal pain: A new concept of nonstructural regional pain," *PAIN Rep.*, vol. 7, no. 5, p. e1024, 2022.

[3] S. Plaut, "Scoping review and interpretation of myofascial pain/fibromyalgia syndrome: An attempt to assemble a medical puzzle," *PLoS ONE*, vol. 17, no. 2, Feb. 2022, Art. no. e0263087.

[4] A. Ojha and D. Kumar, "Psychological factors in fibromyalgia and chronic fatigue syndrome: Implications in counseling," *Bharatiya J. Counselling Psychol.*, vol. 1, no. 1, pp. 1–19, 2021.

[5] H. Ahmad, Y. Gul, S. A. Dawar, Q. Riaz, K. Ullah, and A. Kamal, "Association of depression in patients with fibromyalgia syndrome," *Pakistan J. Med. Health Sci.*, vol. 17, no. 2, pp. 762–765, Apr. 2023.

[6] R. Siracusa, R. D. Paola, S. Cuzzocrea, and D. Impellizzeri, "Fibromyalgia: Pathogenesis, mechanisms, diagnosis and treatment options update," *Int. J. Mol. Sci.*, vol. 22, no. 8, p. 3891, Apr. 2021.

[7] P. Sarzi-Puttini, V. Giorgi, D. Marotto, and F. Atzeni, "Fibromyalgia: An update on clinical characteristics, aetiopathogenesis and treatment," *Nature Rev. Rheumatol.*, vol. 16, no. 11, pp. 645–660, Nov. 2020.

[8] B. Álvarez-Pérez, M. Deulofeu, J. Homs, M. Merlos, J. M. Vela, E. Verdú, and P. Boadas-Vaello, "Long-lasting reflexive and nonreflexive pain responses in two mouse models of fibromyalgia-like condition," *Sci. Rep.*, vol. 12, no. 1, pp. 1–15, Jun. 2022.

[9] L. M. Arnold, D. J. Clauw, and B. H. McCarberg, "Improving the recognition and diagnosis of fibromyalgia," *Mayo Clinic Proc.*, vol. 86, no. 5, pp. 457–464, May 2011.

[10] N. Duda, R. Maguire, I. Gitonga, and S. Corrigan, "Patient and clinician experiences of fibromyalgia, ME/CFS and medically unex-plained symptoms: A meta-aggregative systematic review," *PsyArXiv*, Apr. 2023, doi: 10.31234/osf.io/5ct4k.

[11] C. M. Galvez-Sánchez and G. A. Reyes del Paso, "Diagnostic criteria for fibromyalgia: Critical review and future perspectives," *J. Clin. Med.*, vol. 9, no. 4, p. 1219, Apr. 2020.

[12] D. L. Goldenberg, C. Burckhardt, and L. Crofford, "Management of fibromyalgia syndrome," *Jama*, vol. 292, no. 19, pp. 2388–2395, 2004.

[13] G. Ekici, Y. Bakar, T. Akbayrak, and I. Yuksel, "Comparison of manual lymph drainage therapy and connective tissue massage in women with fibromyalgia: A randomized controlled trial," *J. Manipulative Physiological Therapeutics*, vol. 32, no. 2, pp. 127–133, Feb. 2009.

[14] J. Nijs, O. Mairesse, D. Neu, L. Leysen, L. Danneels, B. Cagnie, M. Meeus, M. Moens, K. Ickmans, and D. Goubert, "Sleep disturbances in chronic pain: Neurobiology, assessment, and treatment in physical therapist practice," *Phys. Therapy*, vol. 98, no. 5, pp. 325–335, May 2018.

[15] T. Giesecke, D. A. Williams, R. E. Harris, T. R. Cupps, X. Tian, T. X. Tian, R. H. Gracely, and D. J. Clauw, "Subgrouping of fibromyalgia patients on the basis of pressure-pain thresholds and psychological factors," *Arthritis Rheumatism*, vol. 48, no. 10, pp. 2916–2922, Oct. 2003.

[16] E. Aksu, E. Berk, A. Sökmen, G. Sökmen, and E. Çelik, "Subclinical cardiac structural and electrical abnormalities in fibromyalgia syndrome," *TURKISH J. Med. Sci.*, vol. 50, no. 4, pp. 885–893, Jun. 2020.

[17] R. J. Thomas, J. E. Mietus, C.-K. Peng, A. L. Goldberger, L. J. Crofford, and R. D. Chervin, ‘‘Impaired sleep quality in fibromyalgia: Detection and quantification with ECG-based cardiopulmonary coupling spectrograms,’’ *Sleep Med.*, vol. 11, no. 5, pp. 497–498, May 2010.
[18] N. AlHinai, ‘‘Introduction to biomedical signal processing and artificial intelligence,’’ in *Biomedical Signal Processing and Artificial Intelligence in Healthcare*. Amsterdam, The Netherlands: Elsevier, 2020, pp. 1–28.
[19] N. Baygin, E. Aydemir, P. D. Barua, M. Baygin, S. Dogan, T. Tuncer, R.-S. Tan, and U. Rajendra Acharya, ‘‘Automated mental arithmetic performance detection using quantum pattern- and triangle pooling techniques with EEG signals,’’ *Exp. Syst. Appl.*, vol. 227, Oct. 2023, Art. no. 120306.
[20] I. Tasci, B. Tasci, P. D. Barua, S. Dogan, T. Tuncer, E. E. Palmer, H. Fujita, and U. R. Acharya, ‘‘Epilepsy detection in 121 patient populations using hypercube pattern from EEG signals,’’ *Inf. Fusion*, vol. 96, pp. 252–268, Aug. 2023.
[21] P. D. Barua, E. Aydemir, S. Dogan, M. A. Kobat, F. B. Demir, M. Baygin, T. Tuncer, S. L. Oh, R.-S. Tan, and U. R. Acharya, ‘‘Multilevel hybrid accurate handcrafted model for myocardial infarction classification using ECG signals,’’ *Int. J. Mach. Learn. Cybern.*, vol. 14, no. 5, pp. 1651–1668, May 2023.
[22] S. Bilgin, E. Arslan, O. Elmas, S. Yildiz, O. H. Colak, G. Bilgin, H. R. Koyuncuoglu, S. Akkus, S. Comlekci, and E. Koklukaya, ‘‘Investigation of the relationship between anxiety and heart rate variability in fibromyalgia: A new quantitative approach to evaluate anxiety level in fibromyalgia syndrome,’’ *Comput. Biol. Med.*, vol. 67, pp. 126–135, Dec. 2015.
[23] M. Kumar, R. Pachori, and U. Acharya, ‘‘Use of accumulated entropies for automated detection of congestive heart failure in flexible analytic wavelet transform framework based on short-term HRV signals,’’ *Entropy*, vol. 19, no. 3, p. 92, Feb. 2017.
[24] T. Nakata, A. Doi, D. Uta, M. Yoshimura, and M.-C. Shin, ‘‘Excessive exercise induces cardiac arrhythmia in a young fibromyalgia mouse model,’’ *PLoS ONE*, vol. 15, no. 9, Sep. 2020, Art. no. e0239473.
[25] J. E. W. Koh, C. P. Ooi, N. S. Lim-Ashworth, J. Vicnesh, H. T. Tor, O. S. Lih, R.-S. Tan, U. R. Acharya, and D. S. S. Fung, ‘‘Automated classification of attention deficit hyperactivity disorder and conduct disorder using entropy features with ECG signals,’’ *Comput. Biol. Med.*, vol. 140, Jan. 2022, Art. no. 105120.
[26] D. Dia, M. Zeghid, T. Saidani, M. Atri, B. Bouallegue, M. Machhout, and R. Tourki, ‘‘Multi-level discrete wavelet transform architecture design,’’ in *Proc. World Congr. Eng.*, vol. 1, 2009, pp. 1–2.
[27] M. Pietikäinen, ‘‘Local binary patterns,’’ *Scholarpedia*, vol. 5, no. 3, p. 9775, 2010.
[28] G. Jacob, R. Sam, H. Geoff, and S. Ruslan, ‘‘Neighbourhood components analysis,’’ in *Proc. Adv. Neural Inf. Process. Syst. (NIPS)*, vol. 17, 2004, pp. 513–520.
[29] H. Liu and R. Setiono, ‘‘Chi2: Feature selection and discretization of numeric attributes,’’ in *Proc. 7th IEEE Int. Conf. Tools Artif. Intell.*, Nov. 1995, pp. 388–391.
[30] L. E. Peterson, ‘‘K-nearest neighbor,’’ *Scholarpedia*, vol. 4, no. 2, p. 1883, 2009.
[31] W. S. Noble, ‘‘What is a support vector machine?’’ *Nature Biotechnol.*, vol. 24, no. 12, pp. 1565–1567, Dec. 2006.
[32] A. Dogan, M. Akay, P. D. Barua, M. Baygin, S. Dogan, T. Tuncer, A. H. Dogru, and U. R. Acharya, ‘‘PrimePatNet87: Prime pattern and tunable q-factor wavelet transform techniques for automated accurate EEG emotion recognition,’’ *Comput. Biol. Med.*, vol. 138, Nov. 2021, Art. no. 104867.
[33] G. Hinton, ‘‘The forward-forward algorithm: Some preliminary investigations,’’ 2022, *arXiv:2212.13345*.
[34] P. D. Barua, A. M. Yildiz, N. Canpolat, T. Keles, S. Dogan, M. Baygin, I. Tuncer, T. Tuncer, R.-S. Tan, H. Fujita, and U. R. Acharya, ‘‘An accurate automated speaker counting architecture based on James Webb Pattern,’’ *Eng. Appl. Artif. Intell.*, vol. 119, Mar. 2023, Art. no. 105821.
[35] A. M. Yildiz, P. D. Barua, S. Dogan, M. Baygin, T. Tuncer, C. P. Ooi, H. Fujita, and U. Rajendra Acharya, ‘‘A novel tree pattern-based violence detection model using audio signals,’’ *Exp. Syst. Appl.*, vol. 224, Aug. 2023, Art. no. 120031.
[36] J. K. Paul, T. Iype, R. Dileep, Y. Hagiwara, J. W. Koh, and U. R. Acharya, ‘‘Characterization of fibromyalgia using sleep EEG signals with nonlinear dynamical features,’’ *Comput. Biol. Med.*, vol. 111, Aug. 2019, Art. no. 103331.
[37] T. Ojala, M. Pietikainen, and T. Maenpaa, ‘‘Multiresolution gray-scale and rotation invariant texture classification with local binary patterns,’’ *IEEE Trans. Pattern Anal. Mach. Intell.*, vol. 24, no. 7, pp. 971–987, Jul. 2002.

PRABAL DATTA BARUA received the Ph.D. degree in information systems from the University of Southern Queensland. He is currently an Academic and Accredited Research Supervisor with the University of Southern Queensland, with 12 years of teaching experience, where he is also an Adjunct Professor. He is an Honourary Industry Fellow with the University of Technology Sydney. He received support from the Queensland Government Innovation Connections under the Entrepreneurs Program to research ‘‘Cancer recurrence using innovative machine learning approaches.’’ He has published several papers in Q1 journals. He is interested in AI technology development in health, education, agriculture, and environmental science. He is an Industry Leader in ICT Entrepreneurship in Australia and an ICT Advisory Panel Member of many organizations.

MAKIKO KOBAYASHI (Senior Member, IEEE) received the B.Eng. and M.Eng. degrees from the Department of Electrical and Electronic Engineering, Chiba University, Japan, in 1997 and 1999, respectively, and the Ph.D. degree from McGill University, Montreal, QC, Canada, in 2004. From 2004 to 2011, she contributed her expertise to the Industrial Materials Institute, a division of the National Research Council of Canada (NRCC). Since 2012, she has been holding an associate professor position with Kumamoto University, where she was promoted to a Professor, in 2022. She has been the Co-Founder and a Technical Advisor of CAST Company Ltd., since 2019. Her research interests include the development of porous piezoelectric materials for high-temperature ultrasonic transducers and various applications. She received the Young Scientist Award from the 26th Symposium on Ultrasonic Electronics, in 2005, and was honored with NRC's 2022 IP Achievement Award.

MASAYUKI TANABE (Member, IEEE) received the Ph.D. degree in engineering from Tokyo Metropolitan University, in 2011. Following the graduation, he has been with the Faculty of Advanced Science and Technology, Kumamoto University, as an Assistant Professor, since 2011. In addition to his academic career, he has ventured into entrepreneurship. His research interests include medical ultrasound imaging and biosignal analysis.

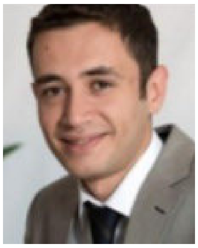

MEHMET BAYGIN received the B.S., M.S., and Ph.D. degrees in computer engineering from Firat University, Elazig, Turkey, in 2010, 2013, and 2018, respectively. He is currently an Assistant Professor with the Department of Computer Engineering, College of Engineering, Erzurum Technical University, Turkey. His research interests include machine learning, computer vision, signal processing, blockchain, and photovoltaic systems.

JOSE KUNNEL PAUL received the MBBS degree from the Government Medical College Thiruvananthapuram, the M.D. degree in general medicine from the Government Medical College, Kottayam, and the DM degree (Hons.) in neurology from the Government Medical College Thiruvananthapuram. He cleared all his entrance examinations in first attempt and secured first rank in Kerala DM entrance examination for neurology. He secured the first rank in the postdoctoral fellowship entrance examination for NIMHANS, Bengaluru. He is a Consultant Neurologist with Holy Family Hospital, Thodupuzha, Kerala. He has published in areas related to fibromyalgia and chronic kidney disease. He is currently working on eosinophilic, bacterial, and tubercular meningitis. He has a passion for clinical neurology, specifically movement disorders and cognitive neurology.

THOMAS IYPE is currently an Emeritus Professor with the Department of Neurology, Medical College Hospital, Thiruvananthapuram. He is an astute clinician and has played a mentoring role for a generation of neurologists across India. He has over 80 published articles and has written 17 book chapters. He has a Research Interest Score of 410.3 (April 7, 2023), 642 citations, and an H-index of 16. He has played a key role in several national and international studies, some of the notable ones being PUREMIND study in India, which is a substudy of PURE Dementia Prevention and Care (DePEC) under the National Institute of Health Research (NIHR) Global Health Group IMPETUStroke (IMPlementation of an Evaluation and Treatment Package for Uniform Stroke Care and Outcomes in the Medical Colleges in India. An Implementation Research Study). His research was funded by ICMR's multicenter national study for which he was Site Principal Investigator). He has received several accolades and awards, including the Certificate of Honor received from the Revised National Tuberculosis Control Programme in Thiruvananthapuram District for outstanding performance and dedication in March 24, 2012, on World TB Day, State Best Doctor Award 2011 in the medical education category, Government of Kerala, and the Master Teachers Award 2020 SHINE 2020.

SENGUL DOGAN received the master's degree in bioengineering and the Ph.D. degree in electrical and electronics engineering from Firat University, Elazig, Turkey, in 2007 and 2011, respectively. She is currently an Associate Professor with the Digital Forensics Engineering, Technology Faculty, Firat University. Her research interests include computer forensics, mobile forensics, image processing, and signal processing. She has been working actively on developing algorithms in machine learning for biomedical data.

TURKER TUNCER received the master's degree in electronics and computer sciences and the Ph.D. degree in software engineering from Firat University, Elazig, Turkey, in 2011 and 2016, respectively. He is currently an Associate Professor with the Digital Forensics Engineering, Technology Faculty, Firat University. His research interests include feature engineering, image processing, signal processing, information security, and pattern recognition. He has been actively working on developing algorithms in machine learning applied to visual surveillance and biomedical data.

RU-SAN TAN is currently a Senior Consultant with the Department of Cardiology, National Heart Centre Singapore. His specialization is in noninvasive diagnostic cardiac imaging: cardiovascular magnetic resonance imaging, echocardiography, and nuclear cardiology. His research interests include advanced cardiac imaging, cardiac biomechanics, and computational modeling. He is a site PI and a member of the steering committees of multinational clinical trials of novel cardiology drugs and notably novel anticoagulants.

U. RAJENDRA ACHARYA received the Ph.D., D.Eng., and DSc degrees. He is currently a Professor with the University of Southern Queensland, Australia; a Distinguished Professor with the International Research Organization for Advanced Science and Technology, Kumamoto University, Japan; and an Adjunct Professor with the University of Malaya, Malaysia and Asia University, Taiwan. His funded research has accrued cumulative grants exceeding six million Singapore dollars. He has authored over 500 publications, including 345 in refereed international journals, 42 in international conference proceedings, and 17 books. He has received more than 72000 citations on Google Scholar (with an H-index of 134). His research interests include biomedical imaging and signal processing, data mining, and visualization, and applications of biophysics for better healthcare design and delivery. He has been ranked in the top 1% of the highly cited researchers for the last seven consecutive years (2016–2022) in computer science, according to the Essential Science Indicators of Thomson. He is on the editorial boards of many journals and has served as the guest editor on several AI-related issues.